

# Damage threshold evaluation of thin metallic films exposed to femtosecond laser pulses: the role of material thickness

G. D. Tsibidis <sup>1,2\*</sup>, D. Mansour <sup>1</sup>, and E. Stratakis <sup>1,3\*</sup>

<sup>1</sup> *Institute of Electronic Structure and Laser (IESL), Foundation for Research and Technology (FORTH), N. Plastira 100, Vassilika Vouton, 70013, Heraklion, Crete, Greece*

<sup>2</sup> *Department of Materials Science and Technology, University of Crete, 71003 Heraklion, Greece*

<sup>3</sup> *Department of Physics, University of Crete, 71003 Heraklion, Greece*

Email: \*[tsibidis@iesl.forth.gr](mailto:tsibidis@iesl.forth.gr); \*[stratak@iesl.forth.gr](mailto:stratak@iesl.forth.gr)

## Abstract

The employment of femtosecond pulsed lasers has received significant attention due to its capability to facilitate fabrication of precise patterns at the micro- and nano- lengths scales. A key issue for efficient material processing is the accurate determination of the damage threshold that is associated with the laser peak fluence at which minimal damage occurs on the surface of the irradiated solid. Despite a wealth of previous reports that focused on the evaluation of the laser conditions that lead to the onset of damage, the investigation of both the optical and thermal response of thin films of sizes comparable to the optical penetration depth is still an unexplored area. In this report, a detailed theoretical analysis of the impact of various parameters such as the photon energies and material thickness on the damage threshold for various metals (Au, Ag, Cu, Al, Ni, Ti, Cr, Stainless Steel) is investigated. A multiscale physical model is used that correlates the energy absorption, electron excitation, relaxation processes and minimal surface modification which leads to the onset of material damage. The satisfactory agreement of the theoretical model with some experimental results indicates that the damage threshold evaluation method could represent a systematic approach towards designing efficient laser-based fabrication systems and optimizing the processing outcome for various applications.

## I. INTRODUCTION

Laser surface processing has emerged as a fast, chemical-free technique for surface patterning and functionalization. In particular, the use of femtosecond (fs) pulsed laser sources for material processing has received considerable attention due to the important technological applications [1-7]. The direct correlation of the response of irradiated solids, the exploration of laser-driven phenomena and the induced surface topographies with potential applications requires a precise knowledge of the fundamental mechanisms that characterise laser-matter interaction. More specifically, a systematic analysis of the ultrafast phenomena that occur ranging from electron excitation to thermalisation of the electron system and transfer of their energy to the lattice is crucial to provide a detailed description of the multiscale processes and enhance the capability to control laser energy towards fabricating application-based topographies. Thus, the elucidation of the complex physical mechanisms appears to be very critical both from a fundamental and application point of view and therefore, consistent methodologies have been developed to explore experimentally and theoretically the multiscale phenomena [8-23].

A key issue for efficient material processing is the accurate determination of the damage threshold that is associated with the laser peak fluence at which minimal damage occurs on the surface of the irradiated solid. With respect to the definition of the damage threshold, two different thermal criteria are usually employed; the first one is associated to the minimum fluence which leads to a phase transition (i.e. maximum lattice temperature exceeds the melting point of the solid) [8, 24] while the second one is related to the minimum fluence that produces temperatures close to the critical temperature that yields material removal [8, 25, 26]. As phase transition or ablation are two processes closely linked with surface patterning, a systematic methodology for the calculation of the damage threshold is desirable. Various, standard and accurate methods for the estimation of the damage threshold have been developed and presented in various reports [27-30]. From a theoretical point of view, the prediction of the damage threshold was performed considering a thermal criterion [8, 24-26] through the use of the classical Two Temperature Model (TTM) [31] which describes the electron-phonon temperature dynamics and relaxation process [32]. Alternative studies also included the employment of atomistic continuum models with the combination of Molecular Dynamics and TTM [20, 32].

Nevertheless, most of the current research focused on the analysis of data aiming to describe damage conditions on bulk materials. Due to the increasing interest in patterning of thin solid films (of sizes comparable to the optical penetration depth) for various applications related to optics, healthcare, sensing, environment, energy [33-43], a detailed investigation of the ultrafast dynamics for such materials is required. Although results have been reported in some previous works for a variety of materials [44-48], a combined theoretical exploration of the multiscale phenomena that take place, the electron excitation, thermal effects, electron-phonon coupling, material damage, the impact of the spectral region of the excitation source for various materials such as noble or transition metals as a function of the material thickness, are still elusive. Results from various experiments have shown that the optical properties of thin materials deviate from those of bulk solids as the thickness decreases to sizes comparable to the optical penetration depth [47]. These results indicate that the level of the absorbed energy will also differ from whether the material is treated as a bulk solid which, in turn, is expected to be reflected on the damage threshold. Similarly, thinner films appear to inhibit the electron diffusion which delays the electron-phonon coupling and leads to lower damage thresholds [44, 46, 47, 49]. On the other hand, it is important to evaluate the opto/thermal response of materials that are classified as noble (such as copper, gold, silver) or transition materials (such as nickel, titanium) whose distinctly different electron distribution [50] appears to affect the optical and thermal properties and therefore, according to the above discussion, the energy absorption is expected to vary at decreasing thickness.

The elucidation of the aforementioned issues through the development of a comprehensive theoretical framework that takes into account processes that have been explored, in principle,

separately is of paramount importance not only to understand the complex physical mechanisms of laser-matter interactions and ultrafast electron dynamics for thin films but also to associate the resulting thermal effects with targeted patterning strategies. To this end, in this work, we present a theoretical model that predicts the damage threshold for various metals (Au, Ag, Cu, Al, Ni, Ti, Cr, Stainless Steel) of increasing thickness (Section II). A library of results is derived through the evaluation of variation of the dielectric parameters as a function of the material thickness through the application of a ‘multiple reflection’ algorithm [51]. A dynamic variation of the optical properties within the pulse duration is also considered which provides appropriate corrections to the excitation level reached by the electron system. Relaxation processes are described through the employment of a TTM and a melting-point-based thermal criterion is used to determine the damage threshold. The investigation has been performed for laser sources at two different spectral regions (515 nm and 1026 nm) to reveal the role of the photon energy in the damage threshold and optical parameters. To validate and assess the model, experimental results for three materials (nickel, chromium, and gold) are tested against theoretical results (Section III). A systematic analysis of the results is illustrated in Section IV while concluding remarks follow in Section V.

## II. THEORETICAL MODEL

To describe the damage induced on the material following irradiation with fs pulses, a theoretical framework is employed to explore the excitation and thermal response of a double-layered structure (thin film/SiO<sub>2</sub>). The simulation algorithm is based on the use of a Two Temperature Model (TTM) that represents the standard approach to evaluate the dynamics of electron excitation and relaxation processes in solids [31]. In this work, for the sake of simplicity, an 1D-TTM is used to describe the thermal effects due to heating of the thin films with laser pulses of wavelength  $\lambda_L=515$  nm and 1026 nm and pulse duration equal to  $\tau_p=170$  fs. Due to the presence of the substrate, the following set of rate equations is employed [52]

$$\begin{aligned}
C_e^{(m)} \frac{\partial T_e^{(m)}}{\partial t} &= \frac{\partial}{\partial z} \left( k_e^{(m)} \frac{\partial T_e^{(m)}}{\partial z} \right) - G_{eL}^{(m)} \left( T_e^{(m)} - T_L^{(m)} \right) + S^{(m)} \\
C_L^{(m)} \frac{\partial T_L^{(m)}}{\partial t} &= \frac{\partial}{\partial z} \left( k_L^{(m)} \frac{\partial T_L^{(m)}}{\partial z} \right) + G_{eL}^{(m)} \left( T_e^{(m)} - T_L^{(m)} \right) \\
C_e^{(S)} \frac{\partial T_e^{(S)}}{\partial t} &= \frac{\partial}{\partial z} \left( k_e^{(S)} \frac{\partial T_e^{(S)}}{\partial z} \right) - G_{eL}^{(S)} \left( T_e^{(S)} - T_L^{(S)} \right) + S^{(S)} \\
C_L^{(S)} \frac{\partial T_L^{(S)}}{\partial t} &= \frac{\partial}{\partial z} \left( k_L^{(S)} \frac{\partial T_L^{(S)}}{\partial z} \right) + G_{eL}^{(S)} \left( T_e^{(S)} - T_L^{(S)} \right)
\end{aligned} \tag{1}$$

where the subscript ‘*m*’ (or ‘*S*’) indicates the thin film (or substrate). In Eqs.1,  $T_e^{(m)}$  and  $T_L^{(m)}$  stand for the electron and lattice temperatures, respectively, of the upper layer. The thermophysical properties of the metal such as the electron  $C_e^{(m)}$  (or lattice  $C_L^{(m)}$ ) volumetric heat capacities, electron  $k_e^{(m)} \left( = k_{e0}^{(m)} \frac{B_e T_e^{(m)}}{A_e (T_e^{(m)})^2 + B_e T_L^{(m)}} \right)$  (or lattice  $k_L^{(m)}=0.01k_e^{(m)}$ ) heat conductivities, the electron-phonon coupling strengths  $G_{eL}^{(m)}$ ,  $A_e$ ,  $B_e$  and other model parameters that appear in the first two equations are listed in Table 1.

The quantity  $S^{(m)}$  represents the source term that accounts for the energy that the laser source gives to the metal surface and it is sufficient to generate excited carriers on the thin film. As the purpose of the present investigation is to reveal the impact of optically excited *thin* films, it is

important to take into account the following processes: (i) a portion of the energy is absorbed in the material while part of the laser energy is transmitted into the substrate, (ii) the reflectivity and transmissivity of the irradiated material are influenced by a *multiple reflection process* between the two interfaces (air/metal and metal/substrate), (iii) the transmitted energy into the substrate does not have sufficient energy to generate excited carriers and therefore, the third equation of Eqs.1 can be removed while the fourth can be simplified by  $C_L^{(S)} \frac{\partial T_L^{(S)}}{\partial t} = \frac{\partial}{\partial z} \left( k_L^{(S)} \frac{\partial T_L^{(S)}}{\partial z} \right)$  where  $T_L^{(S)}$ ,  $C_L^{(S)}$ ,  $k_L^{(S)}$  stands for the substrate temperature, volumetric heat capacity and heat conductivity, respectively. The expression for the source term  $S^{(m)}$  which is used to excite a metallic surface of thickness  $d$  is given from the following formula [47]

$$S^{(m)} = \frac{(1-R-T)\sqrt{4\log(2)}F}{\sqrt{\pi}\tau_p(\alpha^{-1}+L_b)} \exp\left(-4\log(2)\left(\frac{t-3t_p}{t_p}\right)^2\right) \frac{\exp(-z/(\alpha^{-1}+L_b))}{(1-\exp(-d/(\alpha^{-1}+L_b)))} \quad (2)$$

where  $R$  and  $T$  stand for the reflectivity and transmissivity, respectively,  $L_b$  corresponds to the ballistic length,  $\alpha$  is the absorption coefficient that is wavelength dependent, and  $F$  is the peak fluence of the laser beam. The ballistic transport is also included in the expression as it has been demonstrated that it plays significant role in the response of the material [47]. Special attention is required for the ballistic length as in previous works, it has been reported that for bulk materials,  $L_b$  in  $s/p$ -band metals are comparable ( $L_b^{(Au)}=100$  nm,  $L_b^{(Ag)}=142$  nm,  $L_b^{(Cu)}=70$  nm,  $L_b^{(Al)}=46$  nm [47]) while for the  $d$ -band metals such as Ni, Ti, Cr, stainless steel, it is of the same order as their optical penetration depth [47].

The calculation of  $R$  and  $T$  and the absorbance  $A=1-R-T$  are derived through the use of the multiple reflection theory [51]. Thus, the following expressions are employed to calculate the optical properties for a thin film on a substrate (for a  $p$ -polarised beam)

$$R = |r_{dl}|^2, \quad T = |t_{dl}|^2 n, \quad r_{dl} = \frac{r_{am} + r_{ms} e^{2\beta j}}{1 + r_{am} + r_{ms} e^{2\beta j}}, \quad t_{dl} = \frac{t_{am} t_{ms} e^{\beta j}}{1 + r_{am} + r_{ms} e^{2\beta j}}, \quad \beta = 2\pi d / \lambda_L \quad (3)$$

$$r_{CD} = \frac{\tilde{N}_D - \tilde{N}_C}{\tilde{N}_D + \tilde{N}_C}, \quad t_{CD} = \frac{2\tilde{N}_C}{\tilde{N}_D + \tilde{N}_C} \quad (4)$$

where the indices  $C=a,m$  and  $D=m,S$  characterise each material (' $a$ ', ' $m$ ', ' $S$ ' stand for 'air', 'metal', 'substrate', respectively). The complex refractive indices of the materials such as air, metal and substrate are denoted with  $\tilde{N}_a = 1$ ,  $\tilde{N}_m = Re(\tilde{N}_m) + Im(\tilde{N}_m)j$ ,  $\tilde{N}_S = Re(\tilde{N}_S)$ , respectively. Given that soda lime silica glass is used as a substrate material,  $Re(\tilde{N}_S)(\lambda_L = 1026 \text{ nm}) \cong 1.5134$  and  $Re(\tilde{N}_S)(\lambda_L = 515 \text{ nm}) \cong 1.5271$  [53] are the refractive indices of the substrate at the two laser wavelengths used in this work. It is noted that a Drude-Lorentz model is used to obtain the dielectric function for each metal based on the analysis by Rakic *et al.* (where both interband and intraband transitions are assumed) [54]. As the optical parameters of an excited material does not remain constant during the excitation process [21], to introduce the transient change, a temporally varying expression of the dielectric function is provided by including a temperature dependence on the reciprocal of the electron relaxation time  $\tau_e$  (i.e.  $\tau_e = \left[ A_e \left( T_e^{(m)} \right)^2 + B_e T_L^{(m)} \right]^{-1}$ ) [55]. The values of the refractive indices of the metals in this study (at 300 K are given in Table 1).

The volumetric heat capacity of soda lime silica glass is  $C_L^{(S)} = 2.1 \times 10^6 \text{ Jm}^{-3}\text{K}^{-1}$  while the heat conductivity of soda lime silica glass is equal to  $k_L^{(S)} = 1.06 \text{ Wm}^{-1}\text{K}^{-1}$ . The set of equations Eqs.1-4 are solved by using an iterative Crank-Nicolson scheme based on a finite-difference method. It is assumed that the system is in thermal equilibrium at  $t=0$  and, therefore,  $T_e^{(m)}(z, t =$

$0)=T_L^{(m)}(z, t = 0) = 300$  K. A thick substrate is considered (i.e.  $k_L^{(s)} \frac{\partial T_L^{(s)}}{\partial z} = 0$ ) while adiabatic conditions are applied on the surface of the metallic surface (i.e.  $k_e^{(m)} \frac{\partial T_e^{(m)}}{\partial z} = 0$ ). Finally, the following boundary conditions are considered on the interface between the top layer and the substrate:  $k_L^{(m)} \frac{\partial T_L^{(m)}}{\partial z} = k_L^{(s)} \frac{\partial T_L^{(s)}}{\partial z}, k_e^{(m)} \frac{\partial T_e^{(m)}}{\partial z} = 0, T_L^{(m)} = T_L^{(s)}$ .

Parameter	Material							
	Au	Ag	Cu	Al	Ni	Ti	Cr	Steel
$\tilde{N}_m$	DL [54]	DL [55]						
$G_{eL}^{(m)}$ [Wm <sup>-3</sup> K <sup>-1</sup> ]	Ab- Initio [50]	Ab- Initio [50]	Ab- Initio [50]	Ab- Initio [50]	Ab- Initio [50]	Ab- Initio [50]	42×10 <sup>16</sup> [47]	Ab- Initio [56]
$C_e^{(m)}$ [Jm <sup>-3</sup> K <sup>-1</sup> ]	Ab- Initio [50]	Ab- Initio [50]	Ab- Initio [50]	Ab- Initio [50]	Ab- Initio [50]	Ab- Initio [50]	194T <sub>e</sub> <sup>(m)</sup> [47]	Ab- Initio [56]
$C_L^{(m)}$ [×10 <sup>6</sup> Jm <sup>-3</sup> K <sup>-1</sup> ]	2.48 [47]	2.5 [57]	3.3 [47]	2.4 [58]	4.3 [47]	2.35 [59]	3.3 [47]	3.27 [56]
$k_{e0}^{(m)}$ [Wm <sup>-1</sup> K <sup>-1</sup> ]	318 [47]	428 [57]	401 [47]	235 [58]	90 [47]	21.9 [59]	93.9 [47]	46.6 [56]
$A_e$ [×10 <sup>7</sup> s <sup>-1</sup> K <sup>-2</sup> ]	1.18 [57]	0.932 [57]	1.28 [57]	0.376 [58]	0.59 [57]	1 [59]	7.9 [60]	0.98 [56]
$B_e$ [×10 <sup>11</sup> s <sup>-1</sup> K <sup>-1</sup> ]	1.25 [57]	1.02 [57]	1.23 [57]	3.9 [58]	1.4 [57]	1.5 [59]	13.4 [60]	2.8 [56]
$T_{melt}$ [K]	1337 [57]	1234 [57]	1357 [57]	933 [58]	1728 [57]	1941 [59]	2180 [60]	1811 [56]

Table 1: Optical and thermophysical properties of materials (*DL* stands for Drude-Lorentz model).

### III. EXPERIMENTAL PROTOCOL

To determine the damage threshold,  $F_{thr}$ , of thin metal films we used a single shot series of experiment of thin films of various thicknesses. More specifically, Cr metal targets of various thicknesses (10 nm, 20 nm, 40 nm, 100 nm, and 300 nm) and Ni thin films of various thicknesses (10 nm, 20 nm, 40 nm, and 100 nm) were deposited on soda lime silica glass plates of 1 mm thickness by e-beam evaporation [61]. The following experimental setup was used for the calculation of the damage threshold of Ni and Chromium Cr thin films: linearly polarized, Gaussian laser pulses of wavelength of  $\lambda_L = 1026$  nm and pulse duration  $\tau_p = 170$  fs were used for the irradiation of the samples. The laser beam is steered with the help of mirrors, and it was focused, at normal incidence onto the target using a converging lens with focal length equal to  $f = 200$  mm, resulting in a focal spot of waist radius  $w = 28.7 \mu\text{m}$ . In all cases, the samples were placed inside a vacuum chamber, to avoid oxidization of the metals, with constant pressure  $p = 7 \times 10^{-2}$  mbar, the chamber had a window of a fused silica glass plate in order to be transparent to the laser beam which processed the thin metal films.

#### IV. RESULTS AND DISCUSSION

The theoretical model presented in Section II is aimed to describe the dynamics and the response of the electron and lattice subsystems. Given that the objective of the current study is to reveal the impact of the material thickness, firstly, on the absorbed energy and secondly on the thermal response of the material, it is very important to investigate the role and contribution to each component separately.

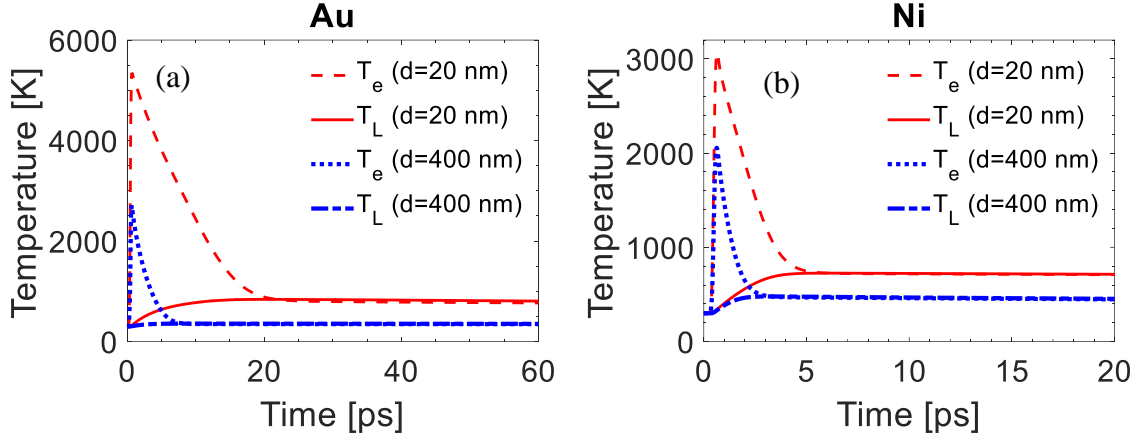


Figure 1: Electron and lattice temperature evolution for (a) Au (20 nm and 400 nm), (b) Ni films (20 nm and 400 nm) ( $\lambda_L=515$  nm).

The ultrafast dynamics following irradiation of two different materials one s/p-band metal (Au) and a d-band metal (Ni) with single laser pulses of  $\lambda_L = 515$  nm was explored while similar conclusions can be deduced for the rest of the metals in this study and at different laser wavelengths. The analysis is, firstly, limited to sub-melting conditions while the study can be also generalised in more extreme conditions. Our simulation results at  $F=10$  mJ/cm<sup>2</sup> for two distinctly different thicknesses, 20 nm and 400 nm, illustrate remarkably contrasting behaviour of the electron and lattice temperatures for the two metals (Figs.1-2). More specifically, for both metals, a decrease of the thickness leads to a smaller depth in which the electrons can diffuse. It is known that the electron subsystem loses energy (cools down) through two competing effects, diffusion and electron-phonon scattering. Due to the fact that electron diffusion is inhibited from small thickness of the film, hot electrons remain confined in a small volume and they lose energy, in principle, through electron-phonon interaction. Therefore, the electron temperature decrease is not as rapid as in the case of a bulk material for both Au and Ni (Fig.1) and the diffusive part in the first equation of Eqs.1 could be ignored. Thus, for small thicknesses, the phonon subsystem will interact with an electron system, which are highly energetic and attain large temperatures. This means that upon relaxation, the produced lattice temperature will be higher than the maximum lattice temperature obtained from the phonon system in thicker materials. Similar results have been reported in previous works as well, however, in those studies approximate values for the thermophysical properties, energy absorption were assumed while the influence of the thickness on the optical properties was ignored [47]; thus, while from a qualitative point of view, the derived results were adequate to present a picture of the ultrafast dynamics, fitting of data were required to correlate the theoretical predictions with experimental observables such as surface modification. Another interesting conclusion from our analysis is that due to the delay in the drop of the electron temperature value, the relaxation of the system will occur at longer times compared with what happens in thicker (or bulk) materials. In Fig.2, the spatiotemporal profile of the lattice temperature field is also illustrated that also shows the enhanced temperature obtained at smaller metal

thicknesses. A comparison of the dynamics and the temperature evolution for the two metals manifests a faster relaxation process for Ni than for Au and this monotonicity holds also for thinner

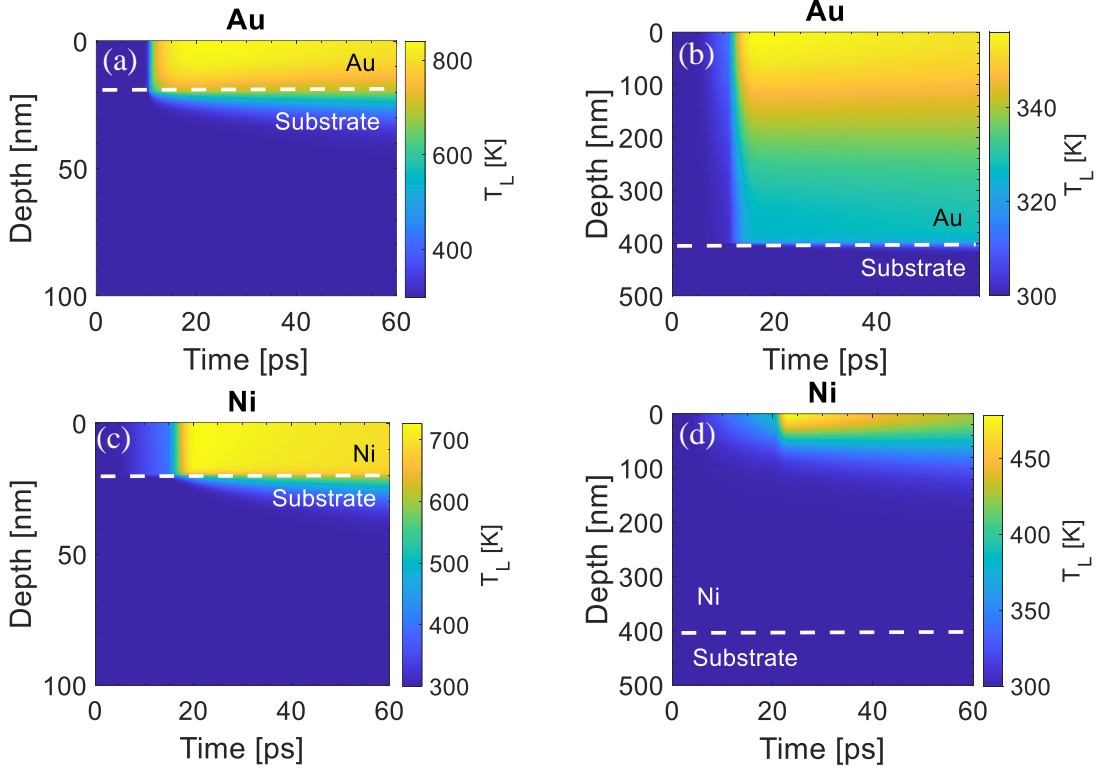


Figure 2: Spatio-temporal lattice temperature evolution for (a) Au (20 nm), (b) Au (400 nm), (c) Ni (20 nm), (d) Ni (400 nm) ( $\lambda_L=515$  nm). The *dashed* white line indicates the interface between the metal and the substrate.

films (Fig.1). This is due to the fact that the electron-phonon coupling for Ni is substantially larger at small temperatures [50] (in principle,  $G_{eL}^{(m)}$  exhibits an opposite monotonicity at increasing electron temperature compared to Au) which accelerates the relaxation process. It is noted that lattice temperature in Au spreads faster in a larger volume (Fig.2b) due to both the larger ballistic electron transport distance and electron diffusion compared to Ni (Fig.2d); this implies an enhanced presence of hot electrons in Au in deeper regions that interact strongly with the phonon system and therefore, larger temperatures are generated inside higher volumes for Au. The above observation is more pronounced for thicker films (Fig2b,d); results do not show a substantial change for thinner films (Fig.2a,c) as the preferential electron diffusion for Au is prevented from the thickness of the material. This behaviour is expected assuming the imposed boundary condition  $k_e^{(m)} \frac{\partial T_e^{(m)}}{\partial z} = 0$  and considering that the transmitted beam is not sufficient to excite the substrate.

The aforementioned discussion about the different thermal response of the material at increasing thickness can be generalised for the rest of the materials in this study. Certainly, a particular emphasis should be made on the distinct behaviour for s/p- band (such as Au, Ag, Cu) and d-band metals (such as Ni, Ti). On the other hand, it is very important to reveal the role of the thickness in the thermal response not only through the inhibited electron diffusion (at smaller thicknesses) and differences in the electron-phonon coupling but also through the variation of the optical response and therefore energy absorption at various thicknesses. Simulations results indicate that there is distinct decrease of the reflectivity for all metals at both laser wavelengths as the thickness size

lowers. More specifically, the theoretical model predicts substantially smaller reflectivity values for thicknesses close to the penetration depth ( $\sim 15\text{-}20$  nm) compared to the values for thicker (or bulk) materials. These results demonstrate the influence of the multiple reflection inside the metal on the optical properties which is strong at small thicknesses (see *left* column in Figs.3-5). Similar conclusions are deduced for the transmissivity and therefore the absorbance inside the upper material (*middle* column in Figs.3-5). To avoid confusion, it is noted that the reflectivity and absorbance values illustrated in Figs.3-5 correspond to the static values at 300 K. However, a transient variation is considered based on the discussion in Section II to evaluate the thermal response of the electron-phonon systems. The theoretical calculations show that the optical properties of the thin film approximate those of the bulk material when the metal thickness is larger than 80 nm. Interestingly, both the reflectivity and absorbance for some metals (i.e. Stainless Steel, Ti, Ni and Cr) demonstrate a small drop from the peak value before they reach a constant evolution at larger thicknesses. This particular behaviour is a characteristic of the dielectric property values of these metals.

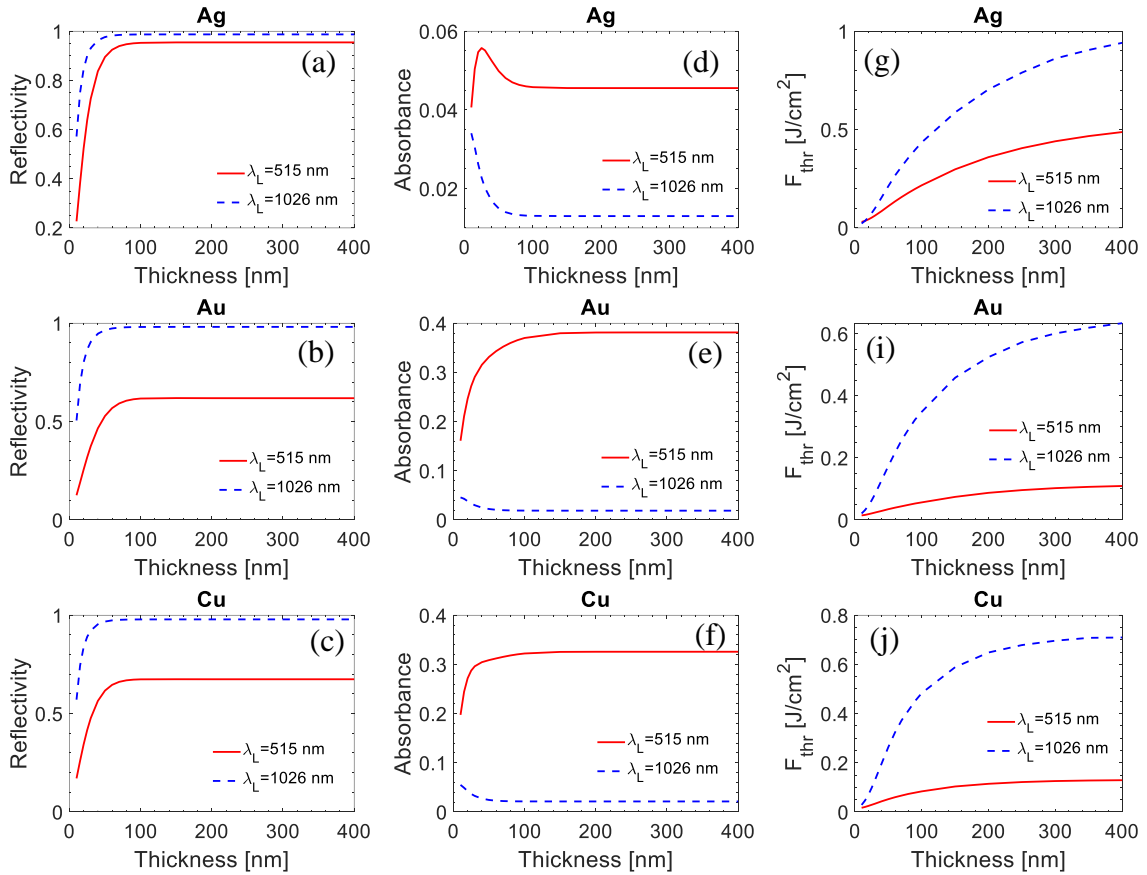


Figure 3: Reflectivity (*left* column), Absorbance (*middle* column) and damage threshold evaluation (*right* column) following irradiation of Au, Ag, Cu with fs laser pulses of two different photon energies ( $\lambda_L=515$  nm and  $\lambda_L=1026$  nm).

An important issue that requires special focus is whether the remarkable deviation of the calculated reflectivity from the standard values measured or predicted for bulk materials (also, confirmed experimentally for various metals at different wavelengths [45]) is expected to affect the thermal response of the material. To investigate the impact of thickness and the produced absorbed energy on the thermal effects, the theoretical framework presented in Section II is employed to describe

the electron dynamics and relaxation processes. The use of the multiscale physical model is aimed to correlate thermal effects with the onset of the material damage. Given that a melting-point-based thermal criterion is chosen to describe the material damage, the objective of the work is the calculation of the minimum (peak) laser fluence that leads to a minimum deformation of the material (i.e. mass displacement).

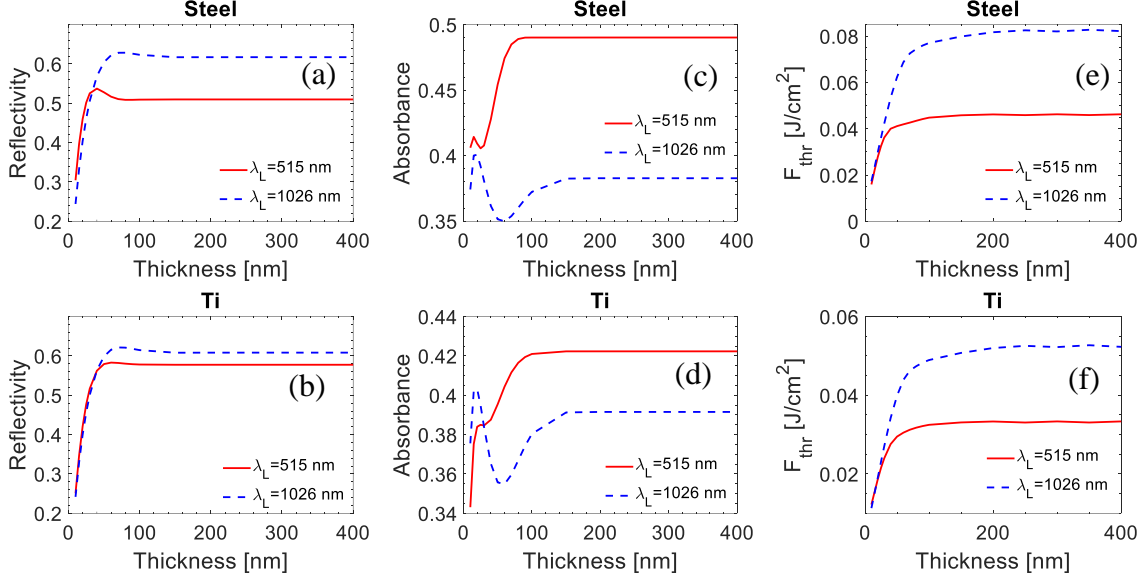


Figure 4: Reflectivity (*left column*), Absorbance (*middle column*) and damage threshold evaluation (*right column*) following irradiation of Steel, Ti with fs laser pulses of two different photon energies ( $\lambda_L=515$  nm and  $\lambda_L=1026$  nm).

Simulations demonstrate an increase of the damage threshold,  $F_{thr}$ , with increasing thickness for all materials (*right column* in Figs.3-5) which is justified from the decrease of the produced lattice temperature on the surface of the material due to, primarily, electron diffusion and ballistic transport (thus, less energetic electrons remain on the surface to interact with the phonon system). This is in agreement with the discussion in the beginning of this section and the fact that electron diffusion is facilitated if the metal thickness increases. On the other hand, results show that there is a threshold value for the thickness  $d_{thr}$  for most metals after which the material behaves more as a bulk solid, a saturation is reached and, therefore, further increase of  $d_{thr}$  does not influence  $F_{thr}$ . Thus, for larger thicknesses,  $F_{thr}$  exhibits an asymptotic behaviour close to the damage threshold of the bulk material. Experimental data in previous reports confirm also this behaviour [44, 46, 48].

Interestingly, the calculations show that for Au, Cu, Ag, Al, the saturation value is delayed while the slow evolution can be attributed to both electron diffusion and the ballistic transport of the hot electrons. Thus, our results show that for most materials, the damage threshold has a linear dependence on film thickness to up to the electron diffusion length  $L_{diff}$  which is  $L_{diff} \sim 400$  nm for Au, Cu, Ag,  $L_{diff} \sim 140$  nm for and  $L_{diff} \sim 50-60$  nm for Stainless Steel, Ni, Ti, Cr (Figs.3-5). A theoretical calculation of the diffusion lengths in previous studies [43] appear to be in good agreement with our simulation results for the damage threshold.

Our simulations for the reflectivity and damage threshold dependence on the metal thickness reveal that there is a discrepancy between the optical and thermal criterion of the definition of a ‘bulk’ material. In the former case, it is related with the minimum thickness of the metal for which the contribution of multiple reflection is not large enough to yield a notably different value from that of the bulk material while the transmissivity is also very small. By contrast, the thermal criterion suggests a higher value of the  $d_{thr}$  at which the material can be described as a bulk metal.

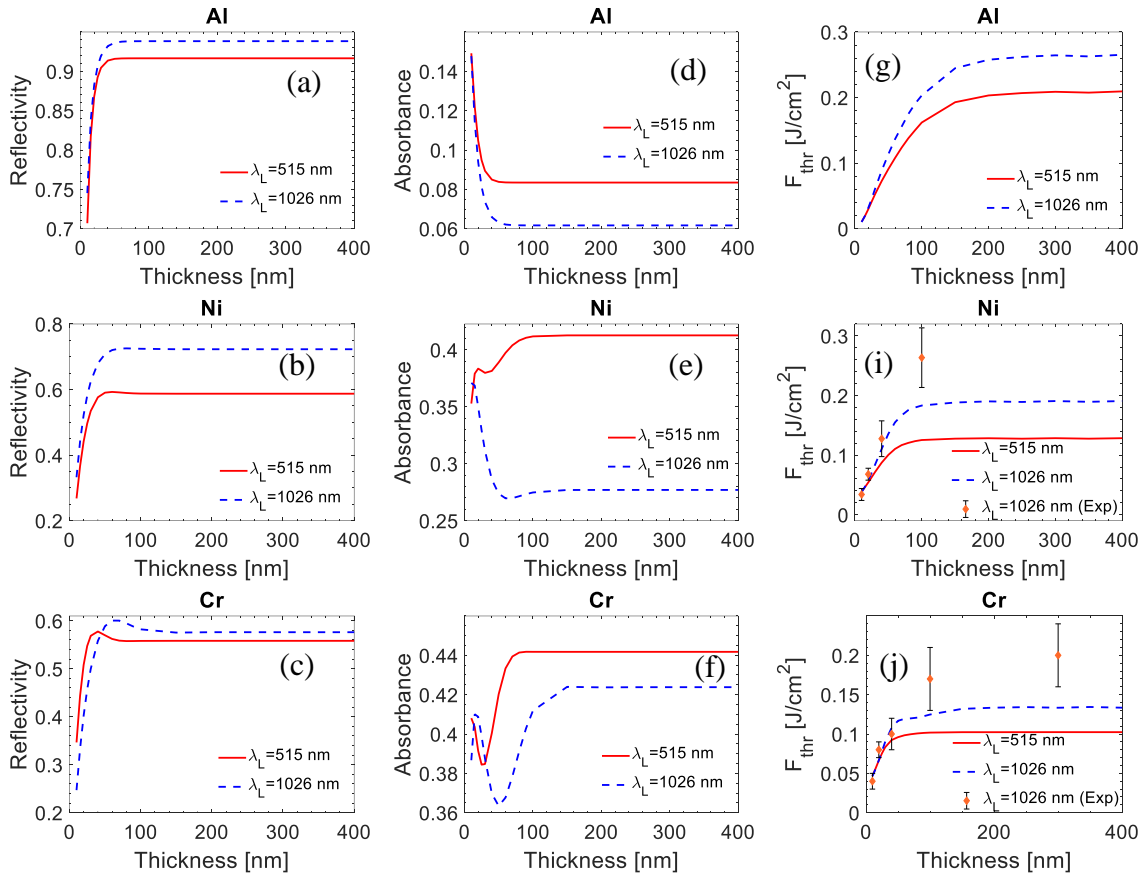


Figure 5: Reflectivity (*left* column), Absorbance (*middle* column) and damage threshold evaluation (*right* column) following irradiation of Al, Ni, Cr with fs laser pulses of two different photon energies ( $\lambda_L=515$  nm and  $\lambda_L=1026$  nm).

The theoretical predictions for the damage threshold presented in this work appear to agree adequately with experimental data in previous reports for irradiation in relatively similar conditions (for Au [44, 48] (see Fig.6 at  $\lambda_L=400$  nm and  $\tau_p=200$  fs) or for Ni [44]). To validate the theoretical framework, an analysis of experimental data obtained in this study has also been performed following irradiation of Ni (Fig.5i) and Cr (Fig.5j) targets of various thicknesses at  $\lambda_L=1026$  nm at  $\tau_p=170$  fs.

For the calculation of single shot damage threshold for Ni and Cr thin films that we used in our experiments, an analysis based in a technique described in Ref. [61] was used. More specifically, the samples were irradiated with a circular beam of waist radius equal to  $w = 28.7 \mu\text{m}$  for various fluence values and the radius of the damaged area was measured. As expected, as the fluence decreases the radius of the defaced area also decreases, thus the fluence threshold,  $F_{thr}$ , was found when the radius of the damaged area reduces to zero. To calculate the peak energy fluence on the sample, the average power of the beam was measured using a power meter placed after the final focusing lens; it is noted that, losses from the fused silica glass plate of the vacuum chamber were estimated to be approximately~6.2%. Figs. 7a,b depict SEM images of samples of Cr and Ni, respectively, showing the circular laser processed area.

It is shown that the theoretical predictions yield a good agreement with the experimental measurements (Figs.5i,j), especially, for small thicknesses. The underestimation for larger thicknesses can be attributed to the fact that the damage threshold criterion used in this report

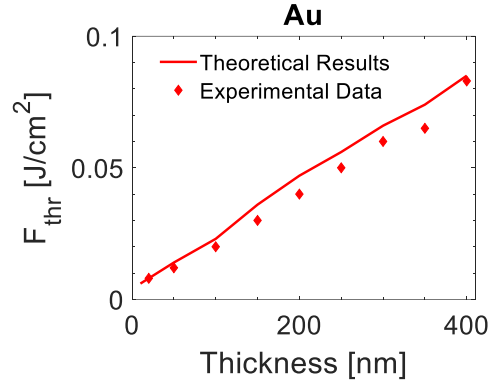


Figure 6: Damage threshold evaluation and comparison with experimental results [42] ( $\lambda_L=400$  nm,  $\tau_p=200$  ps).

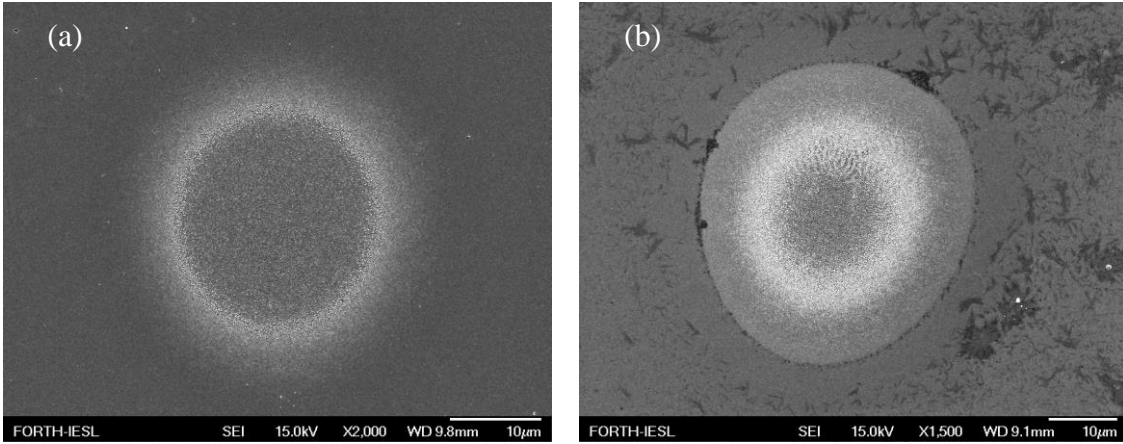


Figure 7: (a) SEM image of a Cr thin film of thickness  $d=100$  nm irradiated with a pulse of peak energy fluence  $F = 0.27$  J/cm<sup>2</sup> resulting in a circular damaged area of radius  $r_D = 22.5$   $\mu$ m. (b) SEM image of a Ni thin film of thickness  $d=100$ nm irradiated with a pulse of peak energy fluence  $F = 0.47$  J/cm<sup>2</sup> resulting in a circular damaged area of radius  $r_D = 26$   $\mu$ m.

assumed that an onset of material damage occurs even if the minimum volume (one pixel of thickness equal to 0.4 nm according to the discretization) exceeds the melting point of the material. As this size is very small to lead to sufficiently large molten volume that can produce stable (and observable) material deformation, a larger fluid volume that can induce a visible surface damage would require an increase of the damage threshold. This implies that an increase in  $F_{thr}$  would provide a better agreement with experimental results. By contrast, for small thicknesses, this discrepancy is not evident due to the fact that the electron diffusion is less pronounced which leads to smaller electron (and lattice) temperature *gradients* inside the volume. Therefore, larger volumes are at a relatively similar temperature, which indicates that for smaller thicknesses it is easier to induce sufficient molten volume that will lead to surface damage. Nevertheless, and in order to be consistent with the widely used definition of the ‘melting-point-based’ damage threshold (which is the minimum value of the peak fluence that yields lattice temperature above the melting point, regardless of how small the molten volume is), a more detailed analysis of the conditions that lead to the production of larger molten volumes is beyond the scope of this work despite the current theoretical framework is still capable to provide a complete analysis.

One aspect that needs to be discussed is the accuracy of the dielectric function expressions that were used for the irradiated solid. As pointed out in the description of the theoretical framework, a Drude-Lorentz model was used to obtain the dielectric function for each metal based on the approach by Rakic *et al.* (where both interband and intraband transitions are assumed) [54]. In that analysis, the oscillator lengths and spectral widths for the Lorentzian terms that are used were obtained through fitting with experimental data and it was assumed that they do not vary during excitation conditions and at higher electron temperatures. On the other hand, the transient character of the dielectric function was introduced through the inclusion of the relaxation time  $\left[ A_e \left( T_e^{(m)} \right)^2 + B_e T_L^{(m)} \right]^{-1}$  [55]. This is an approximate method to present a dynamic behaviour into the optical properties of the material and our simulations show that the assumption yields results for absorbed energy and eventually for the damage threshold that agree with the experimental observations. Nevertheless, a more precise investigation would require the employment of more rigorous approaches that reveal not only a time dependent variation but also an electron temperature dependence of the dielectric properties. Such approaches have been developed that were based on the use of first principles and Density Functional Theories to describe the ultrafast dynamics of various materials ranging from metals [21] to semiconductors [22] and they could be incorporated into a future and more comprehensive revised model.

The emphasis of the current work was on the role of the thickness of an irradiated metal that lies on top of a substrate. Both experimental and theoretical results demonstrated the impact of the thickness both on the optical properties and the damage threshold. The theoretical framework can be generalised for more intricate and interesting (from the point of view of applications) systems where multiple layers are present in which the thermophysical and optical properties of the constituent layers are expected to influence the thermal response of the complex [52, 62, 63]. Furthermore, our results show that the enhanced localisation of the energy transferred into the (for small metal thicknesses), especially for s/p metals for which diffusive transport is otherwise strong, offers a wealth of potential opportunities of nano-patterning.

## V. CONCLUSIONS

A detailed theoretical framework was presented to correlate the impact of the optical properties variation, the damage threshold and the thickness of the most widely used metals for two laser wavelengths of ultrashort laser pulses. It was shown that especially for small thicknesses, the calculated absorbed energy is influenced significantly from the thickness of the irradiated solid, which is reflected on the thermal response of the material. Simulation results which were validated with experimental data on Ni and Cr and data from previous reports (for Au) demonstrated a linear dependence of the damage threshold for thicknesses up to about the optical penetration depth, while at larger thicknesses an asymptotic behaviour close to the damage threshold of the bulk material is presented. By contrast, for s/p-band metals, the significant impact of the electron diffusion and ballistic transport influences significantly the thermal response of the material. The presented model is aimed to provide a tool for an accurate determination of the damage threshold of metals, which is important for a plethora of laser manufacturing approaches.

## ACKNOWLEDGEMENTS

The authors acknowledge support by the European Union’s Horizon 2020 research and innovation program through the project *BioCombs4Nanofibres* (grant agreement No. 862016). G.D.T and E.S. acknowledge funding from *HELLAS-CH* project (MIS 5002735), implemented under the “Action

for Strengthening Research and Innovation Infrastructures” funded by the Operational Programme “Competitiveness, Entrepreneurship and Innovation” and co-financed by Greece and the EU (European Regional Development Fund) while G.D.T acknowledges financial support from COST Action *TUMIEE* (supported by COST-European Cooperation in Science and Technology).

## REFERENCES

- [1] E. Stratakis *et al.*, *Materials Science and Engineering: R: Reports* **141**, 100562 (2020).
- [2] A. Y. Vorobyev and C. Guo, *Laser & Photonics Reviews* **7**, 385 (2012).
- [3] V. Zorba, E. Stratakis, M. Barberoglou, E. Spanakis, P. Tzanetakakis, S. H. Anastasiadis, and C. Fotakis, *Advanced Materials* **20**, 4049 (2008).
- [4] V. Zorba, L. Persano, D. Pisignano, A. Athanassiou, E. Stratakis, R. Cingolani, P. Tzanetakakis, and C. Fotakis, *Nanotechnology* **17**, 3234 (2006).
- [5] J.-C. Diels and W. Rudolph, *Ultrashort laser pulse phenomena : fundamentals, techniques, and applications on a femtosecond time scale* (Elsevier / Academic Press, Amsterdam ; Boston, 2006), 2nd edn.
- [6] E. L. Papadopoulou, A. Samara, M. Barberoglou, A. Manousaki, S. N. Pagakis, E. Anastasiadou, C. Fotakis, and E. Stratakis, *Tissue Eng Part C-Me* **16**, 497 (2010).
- [7] A. Papadopoulos, E. Skoulas, A. Mimidis, G. Perrakis, G. Kenanakis, G. D. Tsibidis, and S. E., *Advanced Materials* **31**, 1901123 (2019).
- [8] G. D. Tsibidis, M. Barberoglou, P. A. Loukakos, E. Stratakis, and C. Fotakis, *Physical Review B* **86**, 115316 (2012).
- [9] G. D. Tsibidis, C. Fotakis, and E. Stratakis, *Physical Review B* **92**, 041405(R) (2015).
- [10] G. D. Tsibidis, E. Stratakis, P. A. Loukakos, and C. Fotakis, *Applied Physics A* **114**, 57 (2014).
- [11] T. J. Y. Derrien, T. E. Itina, R. Torres, T. Sarnet, and M. Sentis, *Journal of Applied Physics* **114**, 083104 (2013).
- [12] J. Z. P. Skolski, G. R. B. E. Romer, J. V. Obona, V. Ocelik, A. J. H. in 't Veld, and J. T. M. De Hosson, *Physical Review B* **85**, 075320 (2012).
- [13] J. Bonse, J. Krüger, S. Höhm, and A. Rosenfeld, *Journal of Laser Applications* **24**, 042006 (2012).
- [14] F. Garrelie, J. P. Colombier, F. Pigeon, S. Tonchev, N. Faure, M. Bounhalli, S. Reynaud, and O. Parriaux, *Optics Express* **19**, 9035 (2011).
- [15] M. Huang, F. L. Zhao, Y. Cheng, N. S. Xu, and Z. Z. Xu, *ACS Nano* **3**, 4062 (2009).
- [16] J. Bonse and J. Kruger, *Journal of Applied Physics* **108**, 034903 (2010).
- [17] G. D. Tsibidis, E. Skoulas, A. Papadopoulos, and E. Stratakis, *Physical Review B* **94**, 081305(R) (2016).
- [18] Y. Shimotsuma, P. G. Kazansky, J. R. Qiu, and K. Hirao, *Physical Review Letters* **91**, 247405 (2003).
- [19] B. N. Chichkov, C. Momma, S. Nolte, F. vonAlvensleben, and A. Tunnermann, *Applied Physics a-Materials Science & Processing* **63**, 109 (1996).
- [20] B. Rethfeld, M. E. Garcia, D. S. Ivanov, and S. Anisimov, *Journal of Physics D: Applied Physics* **50**, 193001 (2017).
- [21] E. Bevilion, R. Stoian, and J. P. Colombier, *Journal of Physics-Condensed Matter* **30**, 385401 (2018).
- [22] G. D. Tsibidis, L. Mouchliadis, M. Pedio, and E. Stratakis, *Physical Review B* **101**, 075207 (2020).
- [23] R. Böhme, S. Pissadakis, D. Ruthe, and K. Zimmer, *Applied Physics A-Materials Science & Processing* **85**, 75 (2006).
- [24] B. Chimier, O. Utéza, N. Sanner, M. Sentis, T. Itina, P. Lassonde, F. Légaré, F. Vidal, and J. C. Kieffer, *Physical Review B* **84**, 094104 (2011).
- [25] G. D. Tsibidis and E. Stratakis, *Sci Rep-Uk* **10**, 8675 (2020).
- [26] I. M. Burakov, N. M. Bulgakova, R. Stoian, A. Rosenfeld, and I. V. Hertel, *Applied Physics a-Materials Science & Processing* **81**, 1639 (2005).
- [27] Y. Jee, M. F. Becker, and R. M. Walser, *Journal of the Optical Society of America B-Optical Physics* **5**, 648 (1988).

- [28] J. Bonse, S. Baudach, J. Kruger, W. Kautek, and M. Lenzner, *Applied Physics a-Materials Science & Processing* **74**, 19 (2002).
- [29] S. Baudach, J. Bonse, J. Kruger, and W. Kautek, *Applied Surface Science* **154**, 555 (2000).
- [30] S. H. Kim, I. B. Sohn, and S. Jeong, *Applied Surface Science* **255**, 9717 (2009).
- [31] S. I. Anisimov, B. L. Kapeliovich, and T. L. Perel'man, *Zhurnal Eksperimentalnoi Teor. Fiz.* **66**, 776 (1974 [Sov. Phys. Tech. Phys. 11, 945 (1967)]).
- [32] D. S. Ivanov and L. V. Zhigilei, *Physical Review B* **68**, 064114 (2003).
- [33] R. Shwetharani, H. R. Chandan, M. Sakar, G. R. Balakrishna, K. R. Reddy, and A. V. Raghu, *Int J Hydrogen Energ* **45**, 18289 (2020).
- [34] A. Piegari and F. o. Flory, *Optical thin films and coatings : from materials to applications*, Woodhead publishing series in electronic and optical materials, number 49.
- [35] K. V. Sreekanth, S. Sreejith, S. Han, A. Mishra, X. X. Chen, H. D. Sun, C. T. Lim, and R. Singh, *Nat Commun* **9**, 369 (2018).
- [36] M. Kumar, M. A. Khan, and H. A. Arafat, *Acs Omega* **5**, 3792 (2020).
- [37] H. Kim, J. Proell, R. Kohler, W. Pflöging, and A. Pique, *Journal of Laser Micro Nanoengineering* **7**, 320 (2012).
- [38] J. Proell, R. Kohler, A. Mangang, S. Ulrich, M. Bruns, H. J. Seifert, and W. Pflöging, *Applied Surface Science* **258**, 5146 (2012).
- [39] J. Proell, R. Kohler, A. Mangang, S. Ulrich, C. Ziebert, and W. Pflöging, *Journal of Laser Micro Nanoengineering* **7**, 97 (2012).
- [40] W. Pflöging, R. Kohler, M. Torge, V. Trouillet, F. Danneil, and M. Stuber, *Applied Surface Science* **257**, 7907 (2011).
- [41] R. Kohler, H. Besser, M. Hagen, J. Ye, C. Ziebert, S. Ulrich, J. Proell, and W. Pflöging, *Microsystem Technologies-Micro- and Nanosystems-Information Storage and Processing Systems* **17**, 225 (2011).
- [42] R. Kohler, P. Smyrek, S. Ulrich, M. Bruns, V. Trouillet, and W. Pflöging, *Journal of Optoelectronics and Advanced Materials* **12**, 547 (2010).
- [43] E. Skoulas, A. C. Tasolamprou, G. Kenanakis, and E. Stratakis, *Applied Surface Science* **541** (2021).
- [44] S. S. Wellershoff, J. Hohlfeld, J. Güdde, and E. Matthias, *Applied Physics A* **69**, S99 (1999).
- [45] J. Hohlfeld, J. G. Müller, S. S. Wellershoff, and E. Matthias, *Applied Physics B-Lasers and Optics* **64**, 387 (1997).
- [46] J. Güdde, J. Hohlfeld, J. G. Müller, and E. Matthias, *Applied Surface Science* **127**, 40 (1998).
- [47] J. Hohlfeld, S. S. Wellershoff, J. Güdde, U. Conrad, V. Jahnke, and E. Matthias, *Chemical Physics* **251**, 237 (2000).
- [48] B. C. Stuart, M. D. Feit, S. Herman, A. M. Rubenchik, B. W. Shore, and M. D. Perry, *J. Opt. Soc. Am. B* **13**, 459 (1996).
- [49] M. Bonn, D. N. Denzler, S. Funk, M. Wolf, S. S. Wellershoff, and J. Hohlfeld, *Physical Review B* **61**, 1101 (2000).
- [50] Z. Lin, L. V. Zhigilei, and V. Celli, *Physical Review B* **77**, 075133 (2008).
- [51] M. Born and E. Wolf, *Principles of optics : electromagnetic theory of propagation, interference and diffraction of light* (Cambridge University Press, Cambridge ; New York, 1999), 7th expanded edn.
- [52] B. Gaković, G. D. Tsibidis, E. Skoulas, S. M. Petrović, B. Vasić, and E. Stratakis, *Journal of Applied Physics* **122**, 223106 (2017).
- [53] M. Rubin, *Sol Energ Mater* **12**, 275 (1985).
- [54] A. D. Rakic, A. B. Djuricic, J. M. Elazar, and M. L. Majewski, *Applied Optics* **37**, 5271 (1998).
- [55] G. D. Tsibidis, A. Mimidis, E. Skoulas, S. V. Kirner, J. Krüger, J. Bonse, and E. Stratakis, *Applied Physics A* **124**, 27 (2017).
- [56] F. Fraggelakis, G. D. Tsibidis, and E. Stratakis, *Physical Review B* **103**, 054105 (2021).
- [57] A. M. Chen, H. F. Xu, Y. F. Jiang, L. Z. Sui, D. J. Ding, H. Liu, and M. X. Jin, *Applied Surface Science* **257**, 1678 (2010).
- [58] B. H. Christensen, K. Vestentoft, and P. Balling, *Applied Surface Science* **253**, 6347 (2007).
- [59] S. Petrovic, G. D. Tsibidis, A. Kovacevic, N. Bozinovic, D. Perusko, A. Mimidis, A. Manousaki, and E. Stratakis, *Eur Phys J D* **75**, 304 (2021).
- [60] A. M. Chen, L. Z. Sui, Y. Shi, Y. F. Jiang, D. P. Yang, H. Liu, M. X. Jin, and D. J. Ding, *Thin Solid Films* **529**, 209 (2013).
- [61] J. M. Liu, *Optics Letters* **7**, 196 (1982).

- [62] S. M. Petrovic, B. Gakovic, D. Perusko, E. Stratakis, I. Bogdanovic-Radovic, M. Cekada, C. Fotakis, and B. Jelenkovic, *Journal of Applied Physics* **114**, 233108 (2013).
- [63] O. V. Kuznetsov, G. D. Tsibidis, A. V. Demchishin, A. A. Demchishin, V. Babzhetsky, I. Saldan, S. Bellucci, and I. Gnilitzky, *Nanomaterials-Basel* **11**, 316 (2021).